Journal of Photonics for Energy

PhotonicsforEnergy.SPIEDigitalLibrary.org

Enhancing silicon solar cells with singlet fission: the case for Förster resonant energy transfer using a quantum dot intermediate

Stefan Wil Tabernig
Benjamin Daiber
Tianyi Wang
Bruno Ehrler

SPIE.

Stefan Wil Tabernig, Benjamin Daiber, Tianyi Wang, Bruno Ehrler, "Enhancing silicon solar cells with singlet fission: the case for Förster resonant energy transfer using a quantum dot intermediate," *J. Photon. Energy* **8**(2), 022008 (2018), doi: 10.1117/1.JPE.8.022008.

Enhancing silicon solar cells with singlet fission: the case for Förster resonant energy transfer using a quantum dot intermediate

Stefan Wil Tabernig,[†] Benjamin Daiber,[†] Tianyi Wang, and Bruno Ehrler[*]
Center for Nanophotonics, AMOLF, Amsterdam, The Netherlands

Abstract. One way for solar cell efficiencies to overcome the Shockley–Queisser limit is downconversion of high-energy photons using singlet fission (SF) in polyacenes like tetracene (Tc). SF enables generation of multiple excitons from the high-energy photons, which can be harvested in combination with Si. In this work, we investigate the use of lead sulfide quantum dots (PbS QDs) with a band gap close to Si as an interlayer that allows Förster resonant energy transfer (FRET) from Tc to Si, a process that would be spin-forbidden without the intermediate QD step. We investigate how the conventional FRET model, most commonly applied to the description of molecular interactions, can be modified to describe the geometry of QDs between Tc and Si and how the distance between QD and Si, and the QD bandgap affects the FRET efficiency. By extending the acceptor dipole in the FRET model to a 2-D plane, and to the bulk, we see a relaxation of the distance dependence of transfer. Our results indicate that FRET efficiencies from PbS QDs to Si well above 50% are possible at very short but possibly realistic distances of around 1 nm, even for QDs with relatively low photoluminescence quantum yield. [DOI: 10.1117/1.JPE.8.022008]

Keywords: energy transfer; quantum dots; silicon; Förster resonant energy transfer; singlet fission; solar cells.

Paper 17117SS received Nov. 7, 2017; accepted for publication Apr. 13, 2018; published online May 10, 2018; corrected Aug. 10, 2019.

1 Introduction

The domination of the solar cell market by silicon led to the search of add-ons that could increase efficiency while also maintaining low cost. One possible way to increase efficiency is by downconverting high-energy light using an organic material that exhibits singlet fission (SF).

In a single-junction solar cell, photons with energy above the bandgap can excite an electron into the conduction band. Excess energy is lost, as the charge carriers quickly thermalize to the band edge. Downconversion schemes minimize the energy lost by thermalization, by converting high-energy photons to lower-energy charge carriers. Downconversion via SF can improve on the single-junction Shockley–Queisser[1,2] efficiency limit, raising it from 33.7% to 44.4%.[3]

SF in organic semiconductors describes the conversion of a singlet exciton into two triplet excitons, conserving spin. In tetracene (Tc), SF is faster (90 ps)[4] than other decay channels, which leads to a yield of almost two triplet excitons per absorbed photon. The resulting triplet excitons cannot relax radiatively to the singlet ground state, as this process is spin-forbidden, leading to a long triplet lifetime. In Tc, the energy of the triplet excitons (1.25 eV)[5] is close to the bandgap of silicon (1.12 eV), allowing in principle for the triplet excitons to be injected into silicon (Si). In one possible realization, the triplet exciton energy is first transferred into a lead

*Address all correspondence to: Bruno Ehrler, E-mail: b.ehrler@amolf.nl

[†]Both authors are contributed equally.

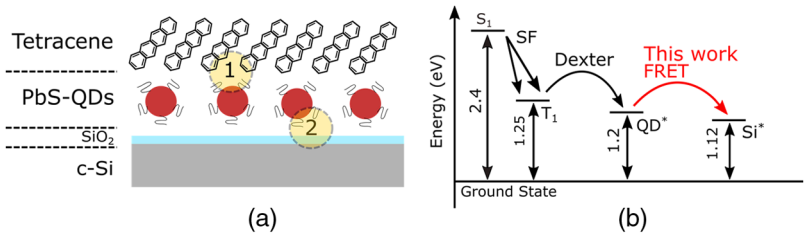

Fig. 1 (a) Illustration of the SF-FRET geometry. A Tc-layer lies on top of the PbS-QD (+ligands) monolayer, which is on top of c-Si. The two yellow circles indicate the two energy transfer steps, namely Tc→QD (1) and QD→Si (2). (b) The Jablonski diagram, with the FRET process between QDs and Si highlighted in red. S_1 and T_1 correspond to the first excited singlet and triplet state in Tc, respectively. The excited states of the QD and Si are indicated by QD* and Si*.

sulphide (PbS) quantum dot (QD)[6] interlayer and subsequently transferred into Si[7,8] (see Fig. 1). Once the triplet exciton is in the QD, the presence of lead with strong spin-orbit coupling leads to intersystem crossing of singlet and triplet states. The spin triplet and singlet excitons are energy degenerate (≈3 meV),[9] which makes the spin mixing efficient. Hence, the exciton can decay radiatively, in principle allowing for energy transfer into Si via photon emission, or Förster resonant energy transfer (FRET). Transfer into lead sulfide[6] and lead selenide[10] QDs was recently demonstrated with high efficiency (>90%).[6] While energy transfer from core/shell CdSe/ZnS QDs into c-Si[7] as well as inter-QD FRET for cases, where energy was transferred among the same QD species[11–13] and between two different QD species,[12,14] has been demonstrated, energy transfer from PbS QDs into Si with a QD bandgap close to the one of c-Si remains to be shown.

One of the processes competing with FRET is the emission of photons by the QDs and the reabsorption in Si. For that process to be efficient, careful light management to funnel photons into silicon is required. In addition, the low external quantum efficiency of the Si cell near the indirect band edge might somewhat limit the achievable efficiency. Direct energy transfer in the form of FRET would be an elegant solution to allow for higher efficiency, as FRET can outcompete radiative energy transfer at distances smaller than the system-specific Förster distance R_0, which is around 8 nm in the case of FRET between PbS QDs.[13,15] Once the exciton resides in Si it will contribute to charge generation, as the extraction efficiency of state-of-the-art Si solar cells is close to unity. Thus, the SF-FRET geometry could lead to additional current in Si solar cells, if short distances between the donor and acceptor can be achieved.

Apart from radiative energy transfer or FRET, other transfer mechanisms are also possible in the Tc-QD-Si geometry. The triplets from Tc could be transferred directly into silicon, bypassing the QDs. This would happen via the Dexter energy transfer mechanism,[8,16] which proceeds via correlated two-electron transfer. In this case, the excited electron of the triplet exciton would be transferred into the excited state in Si, while a ground-state electron from Si transfers into the Tc HOMO. Dexter energy transfer could also act as a transfer channel from the PbS QDs into Si. However, the Dexter transfer efficiency falls exponentially with distance from donor to acceptor due to the required wave function overlap. Thus, Dexter energy transfer is only relevant for short distances <1 nm. The QD ligands already contribute to a ∼1-nm separation between donor and acceptor. Hence, the overall contribution of Dexter energy transfer will presumably be negligible compared to FRET, which has a weaker distance dependency.

Sequential charge transfer from Tc or the PbS QDs to Si is another possible pathway for exciton dissociation, meaning that the electron would be transferred into Si and a hole would transfer from Si into Tc (or vice versa). This mechanism would require sandwiching the active layer between electrodes and is hence undesirable compared to the FRET or Dexter mechanisms.

Here, we establish the theoretical requirements for FRET between PbS QDs and Si, considering the QD bandgap, the distance between Si and QDs, and the geometry of the interface. We find that FRET can be efficient when the QDs are within 3.5 nm to the surface of Si, even for QDs with a bandgap close to the Si bandgap. This is a much shorter distance compared to inter-QD FRET or organic molecules, mostly because the molar absorption coefficient of Si is very low near the band edge. We further find that the distance dependence is somewhat relaxed when considering the Si surface as a plane or bulk acceptor. Finally, we lay out the path

to prepare the Si surface to allow for efficient FRET from Tc into Si. Once efficient transfer of energy between QDs and Si can be achieved experimentally, SF could provide a direct path toward more efficient Si solar cells with minimal need for changes of the Si cell geometry.

2 Förster Resonant Energy Transfer

The FRET efficiency of excitons from QDs into Si, η_{FRET}, is defined in Eq. (1). The main goal of this work is to determine how η_{FRET} depends on donor–acceptor distance on the bandgap of the QDs and on the geometry of the system. The FRET efficiency η_{FRET} compares the FRET rate k_{FRET} to all the competing rates, defined as the exciton decay rate of the QD donor in absence of the silicon acceptor $k_{D,0}$:[17]

$$\eta_{\mathrm{FRET}} = \frac{k_{\mathrm{FRET}}}{k_{D,0} + k_{\mathrm{FRET}}}, \tag{1}$$

where $k_{D,0} = 1/\tau_{D,0}$ and $\tau_{D,0}$ represents the donor exciton lifetime in absence of an acceptor.

FRET is a distance-dependent energy transfer mechanism between two molecules, which are approximated to be point dipoles. Förster derived an expression for the FRET rate,[18] which depends on the emission spectrum of the donor, absorption spectrum of the acceptor, donor lifetime, and donor acceptor distance. The classical as well as quantum mechanical approach both lead to Eq. (2):[17,18]

$$k_{\mathrm{FRET}}(R_{\mathrm{DA}}) = \frac{1}{\tau_{D,0}} \left(\frac{R_0}{R_{\mathrm{DA}}}\right)^6, \tag{2}$$

where R_{DA} represents the distance between donor and acceptor and R_0 is the Förster distance. R_0 determines how strongly the FRET rate depends on the distance and is given by Eq. (3):[17]

$$R_0^6 = \frac{9000\ \ln(10)}{128\pi^5 N_{\mathrm{A}}} * \frac{Q_{\mathrm{D}}\kappa^2 J}{n^4}. \tag{3}$$

In Eq. (3), the prefactor summarizes several numerical constants and Avogadro's number N_{A}. Q_{D} is the donor photoluminescence quantum yield (PLQY), κ^2 is a parameter that depends on the relative orientation between donor and acceptor dipole, and n represents the refractive index of the medium separating donor and acceptor. The parameter J is commonly referred to as spectral overlap integral as it represents the spectral matching of the donor emission and acceptor absorption spectra and is calculated as follows in Eq. (4):[17]

$$J = \int_0^\infty \overline{f_D}(\lambda)\alpha_{M,A}(\lambda)\lambda^4 \mathrm{d}\lambda. \tag{4}$$

The overlap integral contains the normalized emission spectrum of the donor $\overline{f_{\mathrm{D}}}(\lambda)$ and the molar absorption coefficient of the acceptor $\alpha_{M,A}(\lambda)$, integrated over the wavelength λ [gray area in Fig. 2(a)]. We can use the far-field absorption coefficient of silicon for the near-field (Förster) coupling, because FRET has been measured to also be phonon assisted.[7]

Figure 2(a) depicts $\alpha_{M,\mathrm{Si}}$ and $\overline{f_{\mathrm{QD}}}$ as a function of energy. The FWHM assumed for the QD PL is 200 meV, in agreement with literature.[20–22] The refractive index of the separating medium depends on how one accounts for the contributions of the dielectric functions of the QD itself, the surrounding ligand, and the spacer material. Following Yeltik et al.,[7] we consider the average of refractive indices in a straight line from QD to the silicon surface. We approximate the refractive index as constant for different spacer thicknesses. As such, $n_{\mathrm{SiO_2}} = 1.45$ is used, which is the index of the SiO_2 spacer layer in between the QDs and the Si bulk. In fact, the QDs and the ligands will also influence the overall refractive index, as the light will be influenced by an effective medium given that the wavelength of emission is much larger than the distances involved in our system. The refractive index of the QDs is well above 1.45, and the refractive

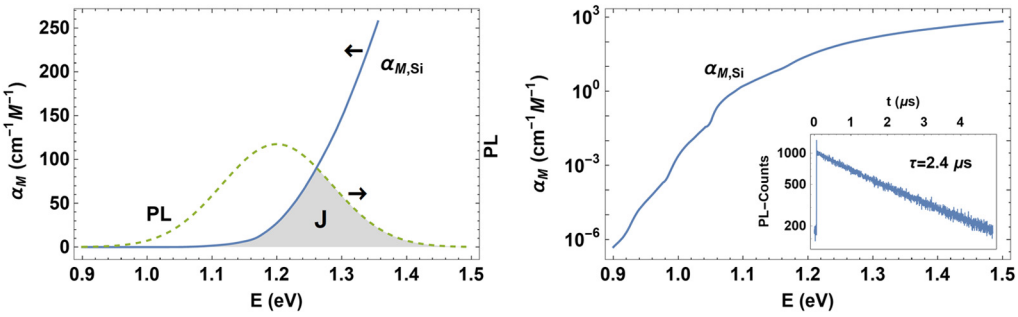

Fig. 2 (a) $\alpha_{M,Si}$ and PL of 1.2 eV PbS QDs as a function of photon energy. The gray shaded area indicates the spectral overlap between the QD donor and the Si acceptor (J). $\alpha_{M,Si}$ was taken from Green and Keevers[19] and the PL spectrum was modeled as a Gaussian centered at 1.2 eV with a FWHM of 200 meV, which corresponds to a broadening of $\sigma = 84$ meV. The PL is scaled by a factor of 25 for visibility. (b) Molar absorption coefficient of silicon $\alpha_{M,Si}$ as a function of photon energy. The inset shows the measured transient PL lifetime for 1.2 eV PbS QDs in solution.

index of the organic ligands is between 1.45 for oleic acid (OA)[23] and 1.5 (3-mercatopropyonic acid)[24] for most organic ligands. Inorganic ligands like ZnI_2 are very short so we can neglect their influence on the electromagnetic field. However, since the ligands do not fill the entire volume,[21] we deem the approximation of $n = 1.45$ valid for distances larger than 1 nm. The orientation parameter κ^2 depends on the relative transition dipole orientation of donor and acceptor.[17] Since the QDs have rotational symmetry, the dipole orientation in the QDs will be isotropic, which yields $\kappa^2_{iso} = \frac{2}{3}$.[17] The quantum yield of PbS-QDs depends on various factors, including size,[25] excitation wavelength,[26] QD concentration,[26] ligands,[27] and whether they are in solution or in solid state. The choice of QD size is important because the corresponding bandgap has to be lower than the Tc triplet exciton energy and higher than the Si bandgap, to ensure that both transfer processes are downhill in energy. We choose QDs with emission centered at 1.2 eV, which corresponds to an average size of 3.4 nm.[25] The PLQY for these QDs ranges from 20% to 55%[26] in solution and up to 15% in films.[28] We determined the radiative lifetime of our 1.2 eV PbS QDs (see experimental methods for details on QD synthesis and PL lifetime measurement) in octane as $\tau_{PbS} = 2.4$ μs [inset Fig. 2(b)], which is in good agreement with literature.[13,20,25] For a more accurate description of the FRET rate, the measured lifetime of the QDs in solution should be replaced by the QD lifetime measured after deposition on quartz, to obtain the reference value for "infinite" donor–acceptor separation $\tau_{D,0}$. We exclude the effects of parasitic absorption in the QD layer because we assume a submonolayer QD coverage. To be specific, the ideal QD coverage to maximize transfer and minimize QD-absorption would be a submonolayer coverage, where the inter-QD spacing is far bigger than the inter-QD Förster radius of 8 nm.[13,15] Making this assumption allows us to neglect any significant contributions of inter-QD FRET. Inter-QD FRET should be regarded as an undesirable decay channel because screening more QDs increases the chance to find a surface trap state, and there will be a tendency to transfer toward lower energy QDs. The upper limit for the QD spacing is determined by the Tc triplet diffusion length. In the final geometry, the QD coverage has to be dense enough to allow all Tc triplets to diffuse toward a QD, meaning that the ideal QD separation corresponds to the triplet diffusion length of around 400 nm.[29,30] Such a QD coverage absorbs less than 0.01% of the solar spectrum, and thus, we can neglect absorption of the incident light by QDs (see Appendix for details on this estimate).

In the following, we calculate R_0, which is the distance for that the transfer efficiency reaches 50% in the dipole–dipole model. While this is not exactly the case for the plane and bulk geometries we will introduce later, R_0 is still a useful quantity to estimate separation distances. As can be seen in the upper plot of Fig. 3, the values for R_0 vary from 0.9 nm to up to 1.5 nm, depending on the QY and bandgap of the QDs. The steep loss of transfer efficiency below the bandgap of silicon (around 1.12 eV) can be attributed to the exponential decrease in the absorption coefficient. The largest QD bandgap for which energy transfer from triplet excitons in Tc was

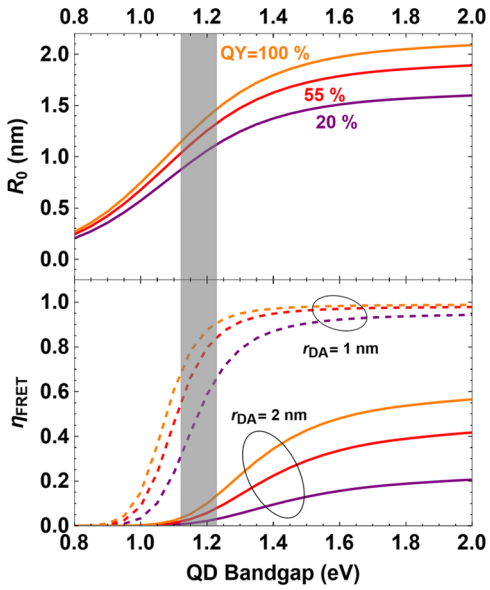

Fig. 3 The upper graph shows the QD bandgap dependence of the Förster distance R_0 for different quantum yields. In the bottom figure, the FRET efficiency as function of QD bandgap is depicted. Dashed lines represent a donor–acceptor distance of 1 nm, solid lines correspond to 2-nm separation. The colors correspond to the same QYs as in the upper figure. The gray shaded region in both plots indicates the bandgap range from 1.12 to 1.23 eV, which is the range relevant for the transfer from Tc into Si.

observed is 1.23 eV,[6] and we indicate the QD bandgap range by the gray area in Fig. 3. The bottom panel of the same figure shows the FRET efficiency, which obeys a relatively steep slope around 1.2 eV, compared to higher bandgaps, suggesting the importance of a careful choice of the QD bandgap. The bottom plot of Fig. 3 shows FRET efficiencies for 1- and 2-nm separation distances, with varying QY. Changes in distance by only 1 nm around R_0 lead to an efficiency increase of up to 75%. The efficiencies at 1-nm separation saturate for bandgaps slightly higher than required in the given geometry at values close to 100%. It is worth noting that high FRET efficiencies (>65%) can be achieved at realistic distances (1 nm) even for a low QY (20%).

3 Influence of Geometry

Up until now, we have calculated the FRET efficiencies according to a dipole–dipole model that does not take into account the extended nature of the silicon acceptor geometry. We introduce two potentially more accurate descriptions of the FRET rate in our system, in the following referred to as "dipole—infinite plane model" and "dipole—bulk model," similar to earlier approaches.[11,31] Our final geometry will probably be best represented by the bulk model, and in the following, we show how it differs from the more conventionally used dipole–dipole description laid out above.

The silicon acceptor occupies one half-space instead of being a point-dipole, leading to a modification of Eq. (2).[32,33] For the dipole-infinite plane model, the zero-dimensional dipole acceptor is substituted with a 2-D acceptor extended over the x-y plane, assuming that the acceptor dipole of FRET mainly resides on the surface of Si [see Eq. (5)]:

$$k_{\mathrm{FRET}} = \sigma_{\mathrm{Si}} \frac{R_0^6}{\tau_{D,0}} \iint_{0,0}^{\infty,2\pi} \frac{r}{(R_{\mathrm{DA}}(r_{\mathrm{DA}}, r))^6} \mathrm{d}r\, \mathrm{d}\phi$$
$$= \sigma_{\mathrm{Si}} \frac{R_0^6}{\tau_{D,0}} \iint_{0,0}^{\infty,2\pi} \frac{r}{\left(\sqrt{r_{\mathrm{DA}}^2 + r^2}\right)^6} \mathrm{d}r\, \mathrm{d}\phi = \sigma_{\mathrm{Si}} \frac{R_0^6}{\tau_{D,0}} * \frac{\pi}{2 r_{\mathrm{DA}}^4}, \quad (5)$$

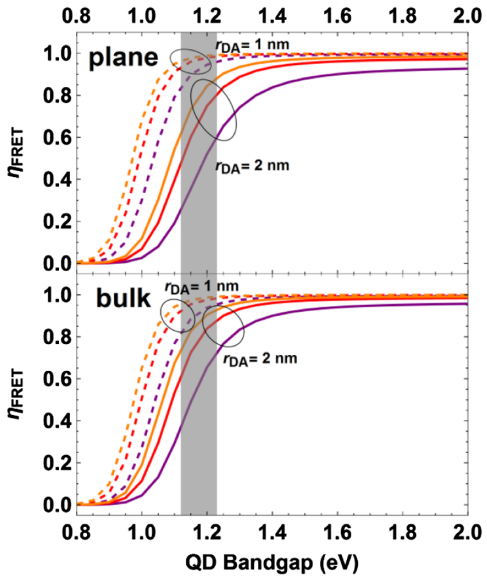

Fig. 4 FRET efficiencies for the "dipole-infinite plane model" (top) and the "dipole-bulk model" (bottom). Dashed and continuous lines represent 1- and 2-nm separation, respectively. The gray shaded region indicates the bandgap range of interest. The colors correspond to the same QY values as in Fig. 3.

where $R_{DA}(r_{DA}, r)$ is the distance from the donor dipole to an infinitesimal acceptor dipole, and σ_{Si} is the density of silicon atoms on a <111> silicon surface ($\sigma_{Si} = 7.8/\text{nm}^2$). After integration over the Si surface (r is the radial component in polar/cylindrical coordinates), the rate only depends on the distance component perpendicular to the surface, thus on r_{DA}. The parameterizations used are illustrated in Fig. 5(b).

While this model is closer to the physical reality, it only considers the Si surface. In order to include the Si bulk, we can simply integrate Eq. (5) over the half space occupied by Si, which leads to Eq. (6):

$$k_{FRET} = \rho_{Si}\frac{\pi R_0^6}{2\tau_{D,0}}\int_0^{-\infty}\frac{1}{(z'(z,r_{DA}))^4}\mathrm{d}z = \rho_{Si}\frac{\pi R_0^6}{2\tau_{D,0}}\int_0^{-\infty}\frac{1}{\left(z\left(\frac{n_{Si}}{n}\right)+r_{DA}\right)^4}\mathrm{d}z$$
$$= \rho_{Si}\frac{\pi R_0^6}{6\tau_{D,0}}\left(\frac{n}{n_{Si}}\right)\frac{1}{r_{DA}^3}. \quad (6)$$

For the integration, $z'(z, r_{DA})$ is split into the integration variable for the half space z and the distance from the donor to the surface of the bulk acceptor r_{DA}, and ρ_{Si} is the density of silicon atoms ($\rho_{Si} = 50/\text{nm}^3$). The additional prefactor $\frac{n}{n_{Si}}$ arises because we have to consider the refractive index of the part of bulk silicon between the infinitesimal acceptor and the QD donor as part of the separating medium. We use a refractive index of 3.55 for silicon n_{Si}, corresponding to the relevant energy region (1.2 eV).[19] For a derivation, see Appendix. We note that the prefactor is independent of distance between donor and acceptor. Mathematically, this is due to the choice of integration limits and leads to an effective Förster distance $R_{0,\text{eff}} = (\frac{n_{SiO_2}}{n_{Si}})^{\frac{1}{6}}R_0$.

Figure 4 shows the FRET efficiencies for both models introduced above. From comparison with the bottom panel of Fig. 3, it becomes obvious that for 2-nm separation, the FRET efficiencies are improved considerably up to around 85% for the dipole—infinite plane model in the relevant region compared to 15% for the dipole—dipole model, whereas the values for 1 nm do not change significantly. This occurs due to the different distance dependencies in different models and acceptor dipole densities (ρ_{Si} and σ_{Si}) in different models, as shown in Fig. 5. Figure 5 shows that the point model shows the steepest distance dependency, which is relaxed in the planar geometry, and the efficiency drop with distance in the bulk model is the most

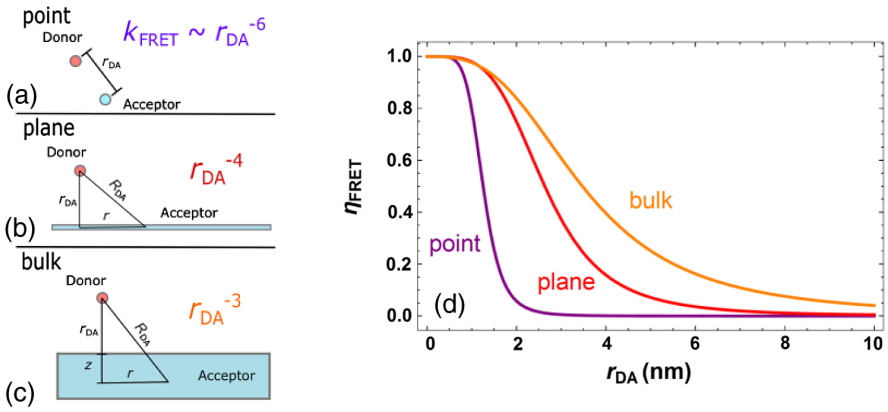

Fig. 5 The three pictures on the left show the three different models [(a) dipole–dipole, (b) dipole–infinite plane, (c) dipole–bulk] and the corresponding donor acceptor distance dependencies obtained by starting from Eq. (2) and integrating over a surface or space. The colors indicate which lines in (d) the dependencies correspond to. (d) The graph shows the FRET efficiency for those three models at distances in the order of R_0. The QD bandgap is 1.2 eV and the QD QY is 55%, corresponding to $R_0 = 1.26$ nm.

shallow. The efficiency is unity for small separations r_{da} for all models and drops of to zero at 2 nm for the point model, 8 nm for the plane model, and is nonzero even for separations exceeding 10 nm for the bulk model.

Usually the characteristic length for FRET, the distance at which the transfer efficiency is 50%, is in the order of 10 nm (QD-QD FRET of 8 nm,[13,15]) which is considerably longer than in the case of QD-silicon energy transfer which we discuss in this paper. However, the FRET distance becomes larger going from point (1.8 nm) to plane (2.5 nm) to bulk (3.5 nm) model. The slope is mainly determined by the distance dependence of the FRET rate [Eq. (1)] which changes from r^{-6} (point model) to r^{-4} (plane model) to r^{-3} (bulk model). The absolute efficiencies going from point to plane to bulk model are larger because the FRET rate is dominant compared to base rate $k_{D,0}$ [Eq. (1)]. The underlying reason for the larger efficiencies is that there are more acceptors available in bulk (ρ_{Si}) compared to plane (σ_{Si}) and point (one acceptor) models.

With increasing distance, first dipole-plane and then dipole-bulk interactions become relatively stronger as they take into account more area/volume. Which model most accurately describes the distance dependence in our QD-silicon geometry? While the bulk-model represents the geometry more accurately, one could argue that due to the strong distance dependence of FRET, the majority of the interaction occurs already at the surface, so the plane-model might be valid after all. However, the spatial extend of the Bloch waves in silicon will ultimately govern the transition geometry.

We note that the mathematical treatment shown here does not take into account that part of the electromagnetic field is reflected by silicon, which leads to a reduced donor lifetime for small distances according to CPS theory.[34] Furthermore, the exciton in the QD could be more accurately described as an extended dipole. The point-dipole approximation is no longer valid if the distance between donor and acceptor is on the order of the exciton (QD) size. If the separation between electron and hole (1.8 nm for PbS QDs[26]) is taken into account, the near field will no longer be accurately described by the r^{-3} dependence used in the FRET derivation. The final step would be the addition of a quantitative description of Dexter transfer,[16] which is a possibly competing charge-mediated energy transfer. Dexter transfer has an exponential distance dependence, which leads to transfer distances of around 1 nm but it does not depend on the absolute molar absorption coefficient of silicon (only on the spectral shape), which could make Dexter rates comparable with FRET rates in this case.

A factor that greatly affects k_{FRET} is the overlap between QD emission and Si absorption spectra. The QD absorption energy must be lower than the Tc triplet exciton energy and the emitted energy of the QD must be above the Si bandgap. The broadening of the QD emission spectrum leads to additional losses when the emission spectrum broadens beyond the given limits. Sharper QD emission spectra could be achieved with a QD ensemble with sharper size

distribution.[35] Apart from that, the Stokes shift might influence the choice of QD size strongly. We now assumed emission at 1.2 eV, which means that the absorption of the QDs would occur at a higher energy. However, the absorption is limited by the fact that Tc triplet states impose an upper boundary for the QD bandgap of around 1.25 eV.

4 Experimental Methods

4.1 *QD Synthesis and Passivation*

The colloidal PbS QDs were synthesized via the hot injection method.[36] In order to obtain the 1.2-eV QDs we measured, the following recipe was followed.[37]

Most chemicals were purchased from Sigma-Aldrich. For those that were not, the distributor will be indicated.

The octadecene is degassed heating to 80°C. A 20-mL syringe is filled with 0.213mL of bis(trimethylsilyl)sulphide (synthesis grade) together with 10 mL of octadecene (technical grade 90%) in a glove box (< 0.5 ppm H_2O, <0.5 ppm O_2) environment. The 0.45 g of PbO (99.999%, Alpha Aesar), 1.34 g of OA (technical grade 90%), and 14.2 g of octadecene are mixed together in a three-necked Schlenk flask. At a temperature of 95°C and under vacuum, this forms a clear solution. Then, the temperature is increased to around 170°C in a nitrogen environment. Now, the Schlenk flask containing the lead precursor is transferred to a heating mantle, which is at room temperature. As soon as the temperature has reached the injection temperature of 150°C (for 1.2-eV QDs), the sulphur precursor is injected into the flask with the solution being vigorously stirred. When the solution has cooled down to 35°C, 20 mL of acetone are added.

For surface passivation with I_2, we follow Lan et al.[38] After the completed synthesis, the QDs are precipitated with acetone in a glovebox. After centrifuging for 4 to 10 min at 4000 to 5000 rpm, the residual liquid is disposed of, which is followed by vacuum-drying of the precipitate overnight. The QDs are then redispersed in toluene (≥99.9%) to obtain a concentration of 150 $\frac{\text{mg}}{\text{ml}}$. Now, a 25-mM iodine (99.999%) in toluene solution is added to the QD solution at a 1∶5 ratio and stirred for 24 h. Afterward, the QDs are precipitated with methanol and centrifuged at 1500 to 5000 rpm for 2 to 5 min. The residual fluid was disposed of, and after a night of vacuum-drying, the QDs were dispersed in octane to obtain a 37.5 $\frac{\text{mg}}{\text{ml}}$ solution.

Eventually, this solution was diluted with octane to obtain a 4.4 $\frac{\text{mg}}{\text{ml}}$ solution, which was used in the lifetime measurements.

4.2 *PL Lifetime Measurement*

The photoluminescence decay of the 1.2 eV bandgap PbS QD was measured on a home-built time-correlated single-photon counting (TCSPC) system consisting of a 640-nm pulsed laser (PicoQuant LDH-D-C-640) with a repetition rate of 0.2 MHz as an excitation source controlled by a PicoQuant PDL 828 "Sepia II." The signal was collected by a single-photon avalanche diode (SPAD) detector (Micro Photon Devices, MPD-5CTD) connected to a PicoQuant HydraHarp 400 multichannel picosecond event timer. The laser has a power of 14.6 μW at the used repetition rate. The laser light was filtered out of the collection path by a Chroma ZET 642-nf notch filter and a Chroma ET 655lp long-pass filter. The TCSPC decays were collected for 5 min.

5 Conclusion

In conclusion, we showed that FRET from PbS QDs to silicon is possible with sufficiently high FRET efficiencies, even for QDs that have a bandgap close to silicon and low PLQY. While efficient FRET is only possible over small separation distances in the order of a few nanometers, those distances are physically feasible, given careful engineering of the interface.

It is of great importance that the emission and absorption peak of the QDs are between the Tc triplet exciton energy and the bandgap of Si, with a narrow emission spectrum.

Hence, to obtain high FRET efficiency for using SF to improve silicon solar cells, a narrow size distribution of adequate QDs leading to a narrow PL peak and to fine tuning of the bandgap and emission yield of the QDs is necessary. Additionally, the silicon surface needs to be passivated electrically and against oxidation with a very thin (sub-nm) layer. Such layers can be achieved with thin metal oxides[39] or self-assembled monolayers of organic molecules.[40] In case of the organic molecules, they could also act as covalent linkers and passivating ligands for the QDs.

Appendix

A.1 Introduction of Bulk Silicon as Additional Separating Medium in the Dipole—Bulk Model

The distance between the QD donor and the infinitesimal dipole acceptor located at an arbitrary spot somewhere in the silicon bulk can be described as $r_{DA} + z = z'$. Here, z' is the total separation distance and r_{DA} and z are the parts in the SiO_2 medium and in silicon, respectively. For simplicity, we now calculate the case for z' perpendicular to the silicon surface (Fig. 6), but the following derivation holds for any angle between the donor–acceptor connection line and the silicon surface.

The total refractive index n_{tot} can be calculated from the effective medium approximation, where n_{tot} is the weighted sum of the two individual indices, for SiO_2 n_{SiO_2} and silicon n_{Si}:

$$n_{tot}(r_{DA} + z) = n_{SiO_2} * r_{DA} + n_{Si} * z.$$

Solving for n_{tot} leads to

$$n_{tot} = \frac{n_{SiO_2} * r_{DA} + n_{Si} * z}{r_{DA} + z} = n_{SiO_2}\left(\frac{r_{DA} + \frac{n_{Si}}{n_{SiO_2}} z}{r_{DA} + z}\right). \tag{7}$$

The obtained expression has to be substituted into a new Förster distance, R_0', following Eq. (3):

$$\begin{aligned} R_0'^6 &= \frac{9000\ \ln(10)}{128\pi^5 N_{AV}} * \frac{Q_D \kappa^2 J}{n_{tot}^4} = \frac{9000\ \ln(10)}{128\pi^5 N_{AV}} * \frac{Q_D \kappa^2 J}{n_{SiO_2}^4} * \left(\frac{r_{DA} + \frac{n_{Si}}{n_{SiO_2}} z}{r_{DA} + z}\right)^{-4} \\ &= R_0^6 * \left(\frac{r_{DA} + z}{r_{DA} + \frac{n_{Si}}{n_{SiO_2}} z}\right)^4, \end{aligned} \tag{8}$$

where R_0 is the ordinary Förster distance for SiO_2 as separating medium. This can now be substituted into the equation for the FRET rate, which we obtained after integration over the surface:

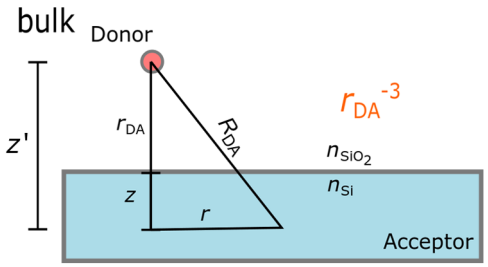

Fig. 6 Illustration of the geometry for the bulk integration of k_{FRET}.

$$k_{\mathrm{FRET}} = \frac{\pi}{2}\int_0^\infty \frac{R_0'^6}{(r_{\mathrm{DA}}+z)^4}\mathrm{d}z = \frac{\pi}{2}R_0^6\int_0^\infty \frac{1}{(r_{\mathrm{DA}}+z)^4}\left(\frac{r_{\mathrm{DA}}+z}{r_{\mathrm{DA}}+\frac{n_{\mathrm{Si}}}{n_{\mathrm{SiO_2}}}z}\right)^4\mathrm{d}z$$
$$= \frac{\pi}{2}R_0^6\int_0^\infty \frac{1}{\left(r_{\mathrm{DA}}+\frac{n_{\mathrm{Si}}}{n_{\mathrm{SiO_2}}}z\right)^4}\mathrm{d}z = \frac{\pi}{2}R_0^6\frac{n_{\mathrm{SiO_2}}}{n_{\mathrm{Si}}}\int_0^\infty \frac{1}{(u)^4}\mathrm{d}u$$
$$= -\frac{\pi}{6}R_0^6\frac{n_{\mathrm{SiO_2}}}{n_{\mathrm{Si}}}\left(0-\frac{1}{r_{\mathrm{DA}}^3}\right) = \frac{\pi}{6}R_0^6\left(\frac{n_{\mathrm{SiO_2}}}{n_{\mathrm{Si}}}\right)\frac{1}{r_{\mathrm{DA}}^3}. \quad (9)$$

The equations above show the derivation of the $\frac{n}{n_{\mathrm{Si}}}$ prefactor in Eq. (6) of the main text. For the integration, substitution of variables was used with $u = r_{DA} + \frac{n_{\mathrm{Si}}}{n}z$.

A.2 Estimate of the Fraction of Light That is Absorbed by the PbS QD Layer

As a conservative estimate, we assume that the QDs are separated by 50 nm on a square lattice, which is well below the triplet diffusion length.[29,30] This means that one QD occupies an area of 50 nm × 50 nm. The QDs are approximated as spheres with a radius of 1.75 nm, which corresponds to a bandgap of 1.2 eV. The volume of the QDs was calculated and divided by the area occupied by one QD, which gives an effective QD layer thickness across the whole geometry of $d_{\mathrm{QD,eff}} = 9 * 10^{-3}$ nm. With this effective layer thickness, we estimated the relative absorption of incident light by the QDs by using the Beer–Lambert law, as shown in Eq. (10):

$$I_{\mathrm{QD}}(\lambda) = I_0(\lambda) * \exp(-\alpha_{\mathrm{QD}}(\lambda)d_{\mathrm{QD,eff}}). \quad (10)$$

Here, $I_{\mathrm{QD}}(\lambda)$ stands for the intensity of light behind the QD layer. $I_0(\lambda)$ is the incident light intensity for which we used the AM1.5 solar spectrum.[41] $\alpha_{\mathrm{QD}}(\lambda)$ denotes the wavelength-dependent absorption coefficient of PbS QDs.[42] The relative intensity loss due to the QDs can then be calculated, as shown in Eq. (11), with the integrals going over the whole wavelength range:

$$\Delta I_{\mathrm{rel}} = \frac{\int (I_0(\lambda) - I_{QD}(\lambda))\mathrm{d}\lambda}{\int I_0(\lambda)\mathrm{d}\lambda}. \quad (11)$$

This leads to a relative intensity loss of $\Delta I_{\mathrm{rel}} = 0.006\%$, which confirms our assumption that QD absorption is negligible in our geometry.

Acknowledgments

This work is part of the research program of The Netherlands Organization for Scientific Research (NWO). The authors thank Ruirt Bosma for the preparation of the PbS QDs and Sven Askes for valuable discussions.

References

1. W. Shockley and H. J. Queisser, "Detailed balance limit of efficiency of p-n junction solar cells," *J. Appl. Phys.* **32**, 510–519 (1961).
2. A. De Vos, "Detailed balance limit of the efficiency of tandem solar cells," *J. Phys. D Appl. Phys.* **13**, 839–846 (1980).
3. M. C. Hanna and A. J. Nozik, "Solar conversion efficiency of photovoltaic and photoelectrolysis cells with carrier multiplication absorbers," *J. Appl. Phys.* **100**, 074510 (2006).
4. M. W. B. Wilson et al., "Temperature-independent singlet exciton fission in tetracene," *J. Am. Chem. Soc.* **135**, 16680–16688 (2013).

5. Y. Tomkiewicz, R. P. Groff, and P. Avakian, "Spectroscopic approach to energetics of exciton fission and fusion in tetracene crystals," *J. Chem. Phys.* **54**, 4504–4507 (1971).
6. N. J. Thompson et al., "Energy harvesting of non-emissive triplet excitons in tetracene by emissive PbS nanocrystal," *Nat. Mater.* **13**, 1039–1043 (2014).
7. A. Yeltik et al., "Phonon-assisted exciton transfer into silicon using nanoemitters: the role of phonons and temperature effects in Förster resonance energy transfer," *ACS Nano* **7**, 10492–10501 (2013).
8. A. Rao and R. H. Friend, "Harnessing singlet exciton fission to break the Shockley-Queisser limit," *Nat. Rev. Mater.* **2**, 17063 (2017).
9. I. Kang and F. W. Wise, "Electronic structure and optical properties of PbS and PbSe quantum dots," *J. Opt. Soc. Am. B* **14**, 1632–1646 (1997).
10. M. Tabachnyk et al., "Resonant energy transfer of triplet excitons from pentacene to PbSe nanocrystals," *Nat. Mater.* **13**, 1033–1038 (2014).
11. M. Lunz et al., "Concentration dependence of Förster resonant energy transfer between donor and acceptor nanocrystal quantum dot layers: effect of donor-donor interactions," *Phys. Rev. B* **83**, 115423 (2011).
12. K. Chou and A. Dennis, "Förster resonance energy transfer between quantum dot donors and quantum dot acceptors," *Sensors* **15**, 13288–13325 (2015).
13. S. W. Clark, J. M. Harbold, and F. W. Wise, "Resonant energy transfer in PbS quantum dots," *J. Phys. Chem. C* **111**, 7302–7305 (2007).
14. C. Wang et al., "Resonant energy transfer between CdSe/ZnS Type I and CdSe/ ZnTe type II quantum dots," *J. Phys. Chem. C* **113**(35), 15548–15552 (2009).
15. A. P. Litvin et al., "Photoluminescence of lead sulfide quantum dots of different sizes in a nanoporous silicate glass matrix," *J. Phys. Chem. C* **121**, 8645–8652 (2017).
16. D. L. Dexter, "A theory of sensitized luminescence in solids," *J. Chem. Phys.* **21**, 836–850 (1953).
17. B. W. Van der Meer, G. Coker, and S.-Y. S. Chen, *Resonant Energy Transfer Theory and Data*, John Wiley & Sons, Inc., New York (1991).
18. T. Forster, "Energiewanderung und fluoreszenz," *Naturwissenschaften* **33**, 166–175 (1946).
19. M. A. Green and M. J. Keevers, "Optical properties of intrinsic silicon at 300 K," *Prog. Photovoltaics* **3**, 189–192 (1995).
20. A. P. Litvin et al., "Size-dependent room-temperature luminescence decay from PbS quantum dots," *Proc. SPIE* **8564**, 85641Z (2012).
21. I. Moreels et al., "Size-tunable, bright, and stable PbS quantum dots: a surface chemistry study," *ACS Nano* **5**, 2004–2012 (2011).
22. C. C. Reinhart and E. Johansson, "Colloidally prepared 3-mercaptopropionic acid capped lead sulfide quantum dots," *Chem. Mater.* **27**, 7313–7320 (2015).
23. B. M. Craig, "Refractive indices of some saturated and monoethenoid fatty acids and methyl esters 1," *Can. J. Chem.* **31** (1961).
24. "Mercaptoacetic acid," http://www.chemicalbook.com/ChemicalProductProperty_EN_CB6477604.htm (6 November 2017).
25. I. Moreels et al., "Size-dependent optical properties of colloidal PbS quantum dots," *ACS Nano* **3**, 3023–3030 (2009).
26. M. Greben, A. Fucikova, and J. Valenta, "Photoluminescence quantum yield of PbS nanocrystals in colloidal suspensions," *J. Appl. Phys.* **117**, 144306 (2015).
27. O. E. Semonin et al., "Absolute photoluminescence quantum yields of IR-26 dye, PbS, and PbSe quantum dots," *J. Phys. Chem. Lett.* **1**, 2445–2450 (2010).
28. G. M. Akselrod et al., "Efficient nanosecond photoluminescence from infrared PbS quantum dots coupled to plasmonic nanoantennas," *ACS Photonics* **3**, 1741–1746 (2016).
29. G. M. Akselrod et al., "Visualization of exciton transport in ordered and disordered molecular solids," *Nat. Commun.* **5**, 1–8 (2014).
30. G. Vaubel and H. Kallmann, "Diffusion length and lifetime of triplet excitons and crystal absorption coefficient in tetracene determined from photocurrent measurements," *Phys. Status Solidi* **35**, 789–792 (1969).
31. P. K. Wolber and B. S. Hudson, "An analytic solution to the Förster energy transfer problem in two dimensions," *Biophys. J.* **28**, 197–210 (1979).

32. M. Stavola, D. L. Dexter, and R. S. Knox, "Electron-hole pair excitation in semiconductors via energy transfer from an external sensitizer," *Phys. Rev. B* **31**, 2277–2289 (1985).
33. J. R. Lakowicz, *Principles of Fluorescence Spectroscopy*, 3rd ed., Springer-Verlag US (2006) .
34. R. R. Chance, A. Prock, and R. Silbey, "Molecular fluorescence and energy transfer near interfaces," *Adv. Chem. Phys.* **37**, 1–65 (2007).
35. B. Hou et al., "Highly monodispersed PbS quantum dots for outstanding cascaded-junction solar cells," *ACS Energy Lett.* **1**, 834–839 (2016).
36. M. A. Hines and G. D. Scholes, "Colloidal PbS nanocrystals with size-tunable near-infrared emission: observation of post-synthesis self-narrowing of the particle size distribution," *Adv. Mater.* **15**, 1844–1849 (2003).
37. R. Bosma, "Size-dependent open-circuit voltage in lead sulfide colloidal quantum dot solar cells," Master Thesis, University of Amsterdam (2017).
38. X. Lan et al., "Passivation using molecular halides increases quantum dot solar cell performance," *Adv. Mater.* **28**, 299–304 (2016).
39. A. Richter et al., "Excellent silicon surface passivation with 5 nm thin ALD Al_2O_3 layers: influence of different thermal post-deposition treatments," *Phys. Status Solidi* **5**, 202–204 (2011).
40. F. Bournel et al., "Adsorption of 2-butyne on Si(0 0 1) at room temperature: a valence band photoemission study," *Surf. Sci.* **601**, 3750–3754 (2007).
41. American Society for Testing and Materials (ASTM), "Terrestrial reference spectra for photovoltaic performance evaluation," *Reference Solar Spectral Irradiance: Air Mass 1.5*, http://rredc.nrel.gov/solar/spectra/am1.5/#about (16 March 2018).
42. Z. Hens and I. Moreels, "Light absorption by colloidal semiconductor quantum dots," *J. Mater. Chem.* **22**, 10406–10415 (2012).

Stefan Wil Tabernig received his bachelor's degree in physics at the Graz University of Technology and then went on to do a master's degree in advanced matter and energy physics at the University of Amsterdam. As part of that, he joined the Hybrid Solar Cells group at AMOLF, 2017, where he is conducting research for his master thesis.

Benjamin Daiber received his bachelor of physics at the University of Heidelberg and his master of physics at the University of Amsterdam. Since 2016 he is a PhD student at AMOLF, Amsterdam, in the Hybrid Solar Cells group of Bruno Ehrler. He is focusing his research on investigating charge carrier dynamics in perovskites and singlet fission materials, like tetracene, and how these insights can inform the design of novel solar cells.

Tianyi Wang received his master's degree in materials science under the Erasmus Mundus master programme master in materials science exploiting large-scale facilities (MAMASELF) in 2014. In December 2014, he joined Hybrid Solar Cell group at AMOLF as a PhD student. His research interests are in synthesizing and understanding photophysics of novel photovoltaic materials.

Bruno Ehrler is leading the Hybrid Solar Cell group at the Institute AMOLF in Amsterdam since 2014. Before he worked as a research fellow at the Optoelectronics group of the Cavendish Laboratory, University of Cambridge. His research interests include organic, quantum dot, and perovskite solar cells.